ACCELERATED PUBLICATION

This paper is available online at www.jbc.org

THE JOURNAL OF BIOLOGICAL CHEMISTRY VOL. 284, NO. 2, pp. 728–732, January 9, 2009

Stromal Interaction Molecule (STIM) 1 and STIM2 Calcium Sensing Regions Exhibit Distinct Unfolding and Oligomerization Kinetics*[S]

Received for publication, September 5, 2008, and in revised form, November 19, 2008
Published, JBC Papers in Press, November 19, 2008, DOI 10.1074/jbc.C800178200

Peter B. Stathopulos[1,2], **Le Zheng**[1], **and Mitsuhiko Ikura**[3]

From the Division of Signaling Biology, Ontario Cancer Institute and Department of Medical Biophysics, University of Toronto, Toronto, Ontario M5G 1L7, Canada

Stromal interaction molecules (STIM) 1 and STIM2 are regulators of store-operated calcium (Ca^{2+}) entry as well as basal cytoplasmic Ca^{2+} levels in human cells. Despite a high sequence similarity (>65%) and analogous sequence-based domain architectures, STIM1 and STIM2 differentially influence these phenomena. Among all eukaryotes, the endoplasmic reticulum luminal portion of STIM proteins minimally encode EF-hand and sterile α-motif (SAM) domains (EF-SAM), which are responsible for sensing changes in Ca^{2+} levels and initiating oligomerization. STIM oligomerization is a key induction step in the activation of Ca^{2+}-permeable channels on the plasma membrane. Here, we show that the kinetic half-time of conversion from a monomeric to a steady oligomeric state is >70× shorter for STIM1 EF-SAM than STIM2 under similar conditions. Urea-induced rates of unfolding for STIM1 EF-SAM are >3× quicker when compared with STIM2, coherent with partial unfolding-coupled aggregation. Additionally, we demonstrate that the isoform-specific N-terminal residues beyond EF-SAM can influence the stability of this region. We postulate that distinct oligomerization dynamics of STIM isoforms have evolved to adapt to differential roles in Ca^{2+} homeostasis and signaling.

Calcium is an essential signaling messenger in every eukaryotic cell, regulating diverse and kinetically distinct cellular phenomena (1). Cytoplasmic Ca^{2+} entry occurs in these cells via two non-mutually exclusive mechanisms with distinguishable spatio-temporal characteristics; 1) transient elevation takes place via Ca^{2+} efflux from the endoplasmic reticulum (ER)[4] luminal stores, and 2) sustained Ca^{2+} influx ensues from the extracellular space. The link between these processes is termed store-operated Ca^{2+} entry (SOCE) and is a major Ca^{2+} entry pathway in eukaryotic cells (2, 3). Receptor-stimulated inositol 1,4,5-triphosphate production induces ER Ca^{2+} store depletion, which signals activation of highly Ca^{2+}-selective channels on the plasma membrane (PM), providing the sustained influx to the cytoplasm. SOCE is crucial to modulating a litany of regulatory processes including gene expression, protein folding, and initiation of cell death pathways (1).

The two principal molecular components of SOCE have been established with STIM1 as the ER Ca^{2+} sensor and activator of Ca^{2+}-selective PM channels (4, 5) and Orai1 as a major component of the PM channel pore (6–10). STIM proteins are type-I transmembrane proteins. The ER luminal N-terminal region of STIM1 includes an ER signal peptide, an EF-hand pair, and a SAM domain, whereas the cytosolic portion consists of two coiled-coil domains, a Pro/Ser-rich region, and a Lys-rich region (11, 12). STIM2, a mammalian homologue, deviates from STIM1 in sequence similarity at the C-terminal end (11, 13).

ER-resident STIM1 redistributes into aggregates in close apposition to the PM (punctae) upon luminal Ca^{2+} depletion (14–17). This punctae formation is causal for Orai1 accumulation at apposing sites in the PM and opening of store-operated Ca^{2+} (SOC) channels at these ER-PM regions of STIM1-Orai1 co-localization (16). Ca^{2+} depletion-induced oligomerization of STIM occurs prior to accretion at ER-PM junctions (17). The luminal portion of STIM provides the structural machinery required for Ca^{2+} sensing as EF-hand Ca^{2+} binding mutants form punctae constitutively (5, 14, 18, 19) and SAM deletion mutants lack the ability to form inducible punctae (20). Replacing EF-SAM in STIM1 with the FK506- and rapamycin-binding protein (FKBP12) or FKBP-rapamycin binding (FRB) domain of mammalian target of rapamycin allows for rapamycin analogue-induced oligomerization and SOCE control independent of luminal Ca^{2+} (21). Recently, we determined the solution structure of STIM1 EF-SAM, which revealed that destabilization of the EF-hand-SAM domain intramolecular interaction is central to oligomerization of this luminal portion of STIM1 (12). The cytosolic C-terminal portion of STIM1 is indispensable for translocation to ER-PM junctions and activation of SOC channels (17, 20, 22, 23).

The function of STIM2 is more complex than STIM1 with some data suggesting no effect on SOCE, whereas other data show Ca^{2+} store-dependent and -independent roles in the inhibition and activation of SOCE as well as maintenance of basal cytoplasmic and luminal Ca^{2+} levels (4, 5, 13, 18, 24–26). Swapping a portion of the STIM1 canonical EF-hand loop with that of STIM2 produces STIM2-like Ca^{2+} sensitivity from the STIM1 mutant in intact cells (26), implying a crucial role for the luminal region in mediating functional disparities between iso-

* This work was supported by a Canadian Institutes of Health Research operating grant and by Canadian Foundation for Innovation funding for 800 and 600 MHz NMR spectrometers. The costs of publication of this article were defrayed in part by the payment of page charges. This article must therefore be hereby marked "*advertisement*" in accordance with 18 U.S.C. Section 1734 solely to indicate this fact.

[S] The on-line version of this article (available at http://www.jbc.org) contains two supplemental figures.

[1] Both authors contributed equally to this work.

[2] Funded through Natural Sciences and Engineering Research Council and Knudson fellowships.

[3] Holds the Canada Research Chair in Cancer Structural Biology. To whom correspondence should be addressed: MaRS Toronto Medical Discovery Tower, Rm. 4-804, 101 College St., Toronto, ON, Canada M5G 1L7. Tel.: 416-581-7550; Fax: 416-581-7564; E-mail: mikura@uhnres.utoronto.ca.

[4] The abbreviations used are: ER, endoplasmic reticulum; STIM, stromal interaction molecule; SOCE, store-operated Ca^{2+} entry; SOC, store-operated Ca^{2+}; SAM, sterile α-motif; PM, plasma membrane; SLS, static light scattering; DLS, dynamic light scattering.

forms. Here, we reveal fundamental differences in the oligomerization dynamics of the EF-SAM portions of STIM1 and STIM2, which may contribute to the distinctions observed in the Ca^{2+}-sensing abilities of the mammalian homologues in the regulation of Ca^{2+} influx and homeostasis.

EXPERIMENTAL PROCEDURES

Recombinant Protein Expression—Human *STIM1* and *STIM2* genes were from Origene Technologies, Inc. The STIM1 EF-SAM construct encoded residues Ser-58–Gly-201, STIM2 EF-SAM encoded Thr-62–Gly-205, long-N STIM1 encoded Leu-23–Asp-213, and long-N STIM2 encoded Cys-15–Gly-205, where residue numbering is consistent with Fig. 1*A*. Recombinant expression and purification was carried out as described previously for Ca^{2+}-loaded and -depleted proteins (27, 28). All experiments were performed in 20 mM Tris-HCl (pH 7.5) containing 100 mM NaCl, supplemented with 0.5 mM EDTA or 5 mM $CaCl_2$ for Ca^{2+}-free and -loaded samples, respectively. Protein concentrations were calculated using $\epsilon_{280\,nm}$ = 1.54, 1.40, 1.24, and 1.13 (mg ml^{-1}) cm^{-1} for STIM1 EF-SAM, STIM2 EF-SAM, long-N STIM1, and long-N STIM2, respectively.

Far-UV CD—Far-UV CD spectra were recorded on a Jasco J-815 CD spectrometer (Jasco, Inc.). Data were collected using 0.01–0.2-cm path length ES quartz cuvettes. Wavelength scan rates were at 20 nm min^{-1} with a response time of 8 s and bandwidth of 1 nm. Thermal melts were acquired in 1 °C-increments at a scan rate of 1 °C min^{-1}. Kinetics of unfolding was monitored in 60-s increments (8-s response) for 4200 s through 0.1–0.2-cm path lengths.

Fluorescence Spectroscopy—Urea-induced unfolding was monitored by changes in intrinsic fluorescence emission at 330 nm induced by excitation light at 280 nm on a Shimadzu RF-5301PC fluorometer (Shimadzu Corp.). Samples were in 1-ml (1-cm path length) ES quartz cuvettes. Excitation and emission slit widths were 1.5 and 10 mm, respectively. Integration time was set to 0.25 s over the 300-s time course. Kinetics were non-linearly fit to a single exponential decay with a sloping baseline,

$$y = A\exp^{(-kx)} + mx + b \qquad \text{(Eq. 1)}$$

where y is the fluorescence signal, A is the absolute change in fluorescence, k is the unfolding rate constant (k_{unf}), m is the slope of the unfolded baseline, b is the intercept of the unfolded baseline, and x is time.

Static and Dynamic Light Scattering (SLS/DLS)—Light scattering measurements were made with a Dynapro DLS module (Wyatt Technologies, Inc.) using a scattering angle of 90° and incident laser light of 825 nm. Samples (0.2-ml) were in 0.3-cm ES quartz cuvettes or 1.0-cm UVettes (Eppendorf AG). SLS intensity was collected every 3–10 s (3–10-s averaging time) over each time course. The average of the first and last 10 consecutive correlation functions (10 s of averaging time each) for the $t = \sim 0$ and $t = \sim 5000$ s distribution of hydrodynamic radii, respectively, was employed for deconvolution using the accompanying DYNAMICS software (Wyatt Technologies, Inc.).

RESULTS

EF-SAM undergoes Ca^{2+} depletion-dependent oligomerization (27, 28), where the stability of the EF-hand-SAM intramolecular interaction is fundamental to this Ca^{2+}-sensing mechanism (12). Because the EF-hand and SAM domains are minimally conserved among all species-specific STIM proteins (29) (Fig. 1*A*), investigating the aggregation characteristics of EF-SAM isoforms may shed light on the basis for differences in STIM function. Here, we assessed the EF-SAM oligomerization kinetics in a Ca^{2+}-free context to gain further insight into the functional disparities between STIM1 and STIM2.

STIM1 EF-SAM Unfolds Faster than STIM2—Oligomerization of EF-SAM is coupled with partial unfolding as a loss in α-helicity is observed concomitant with an increase in random coil and aggregation upon Ca^{2+} depletion (27). The time-dependent loss in helical structure was used as a kinetic probe to oligomerization by monitoring far-UV CD at 225 nm. Ca^{2+}-depleted STIM1 EF-SAM shows no time dependence on the loss in α-helicity as the CD signal is unchanged at high and low protein concentrations (Fig. 1*B*). In contrast, STIM2 EF-SAM undergoes a much slower change from a highly α-helical state to a conformation that resembles STIM1 EF-SAM (low α-helicity). The kinetics for STIM2 EF-SAM exhibits a protein concentration dependence with the highest concentration undergoing the fastest transformation (Fig. 1*B*).

To assess whether the oligomerization-coupled partial unfolding rates are consistent with the inherent unfolding ability of these isoforms, we measured the denaturant-induced unfolding kinetics using intrinsic fluorescence. The urea-induced unfolding curves were well fit to a single exponential (Fig. 1*C*); the apparent single phase is consistent with the two-state equilibrium data previously reported for EF-SAM and the folding of EF-SAM as a single structural entity (27). The unfolding rate of STIM1 EF-SAM was ~3.5–4-fold faster than STIM2 over the range of urea concentrations tested (2.25–3.25 M) (Fig. 1*C*, *inset*). The faster rate of unfolding implies that STIM1 EF-SAM more readily accesses the aggregation-coupled partially unfolded state than STIM2 and is coherent with the markedly quicker oligomerization-coupled unfolding observed in Fig. 1*B*.

STIM2 EF-SAM Aggregates Show a Distribution of Hydrodynamic Radii Similar to STIM1—DLS was employed to assess the distribution of hydrodynamic radii for the EF-SAM isoforms as a function of time. The inherently oligomeric distribution of radii centered at ~7–10 nm does not change with time for STIM1 (Fig. 2*A*), whereas STIM2 EF-SAM solutions evolve from monomers of ~2 nm to oligomers of ~5–10 nm resembling STIM1 (Fig. 2*B*). STIM2 EF-SAM aggregation kinetics is protein concentration-dependent (Fig. 2*D*) as observed for the coupled unfolding (Fig. 1*B*), whereas STIM1 is aggregated independent of protein concentration (Fig. 2*C*). The SLS intensity of aggregated STIM2 EF-SAM is greater than STIM1 at the highest protein concentration, indicating that although the bulk of the oligomers have similar hydrodynamic radii (Fig. 2, *A* and *B*), STIM2 forms a greater percentage of larger aggregates, which contributes the majority of the SLS intensity. The non-linearity in SLS intensity *versus* size precludes the fitting of meaningful rate constants.

To confirm that the Ca^{2+}-free aggregation propensities are retained under more physiological circumstances, we reassessed the kinetics starting from a Ca^{2+}-loaded monomeric state at 37 °C. Upon the addition of 50 mM EDTA to EF-SAM in 5 mM $CaCl_2$, the SLS intensity abruptly began to increase for

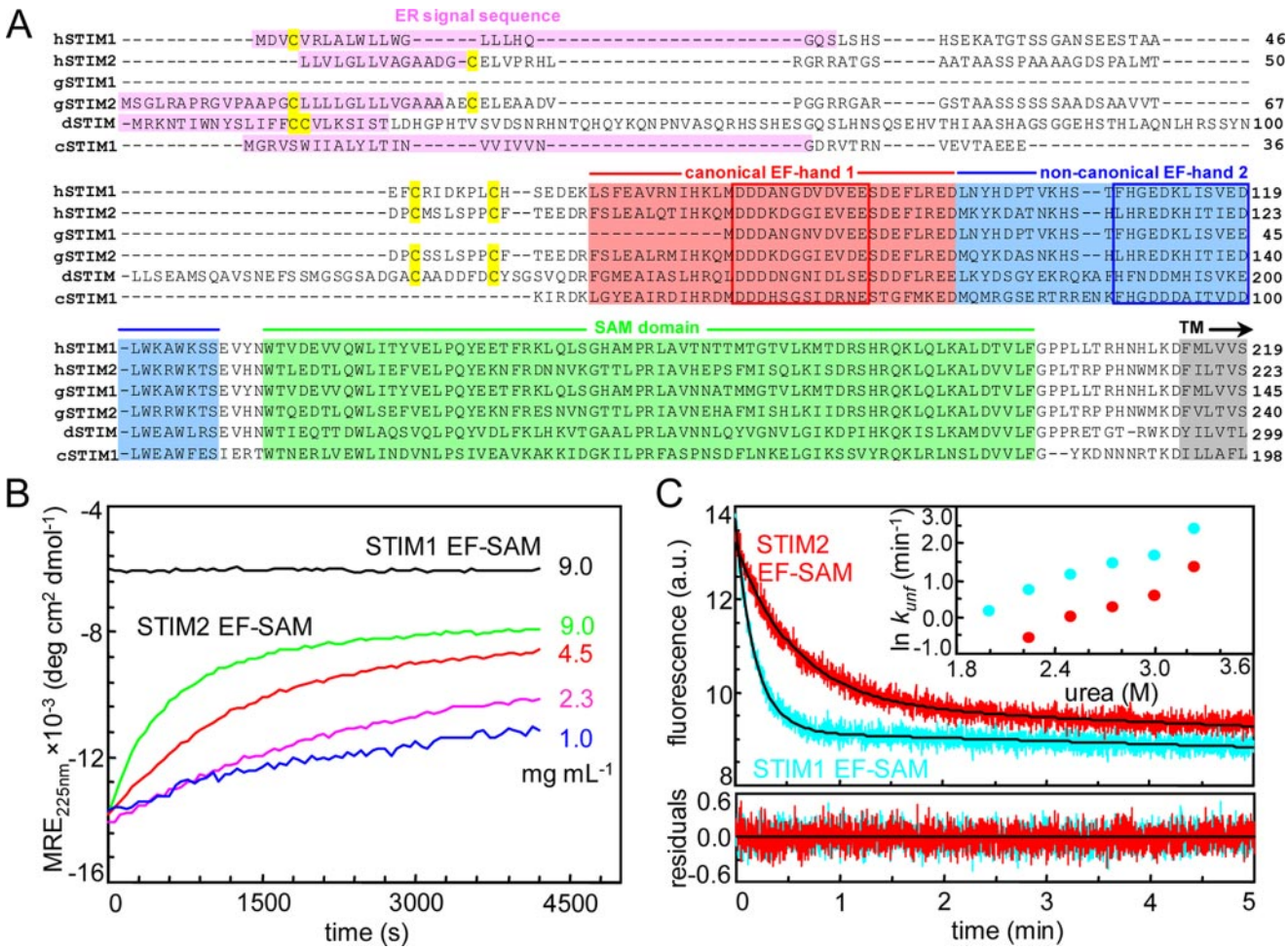

FIGURE 1. **EF-SAM sequence homology and unfolding rates.** *A*, sequence alignment of the luminal domains of STIM isoforms. Alignment for *Homo sapiens* STIM1 (*hSTIM1*; accession NM_003156), *H. sapiens* STIM2 (*hSTIM2*; NM_020860), *G. gallus* (*gSTIM1*; NM_001030838), *G. gallus* STIM2 (*gSTIM2*; XM_420749), *D. melanogaster* (*dSTIM*; AF328906), and *C. elegans* (*cSTIM1*; NM_001027745) was performed using ClustalW. The predicted ER signal sequences are shaded in *purple* (35). Canonical EF-hand 1 residues are shaded *red*, non-canonical EF-hand 2 residues are *blue*, the SAM domain is *green*, and the predicted transmembrane (*TM*) is *gray*. EF-hand loop residues are bounded by *boxes*, and all cysteine residues are shaded *yellow*. *B*, aggregation-coupled unfolding for STIM1 and STIM2 EF-SAM. Ca^{2+}-depleted samples were initially incubated at 4 °C; unfolding was monitored as the decrease in mean residue ellipticity (*MRE*) at 225 nm upon switching to 25 °C. The persistently aggregated and partially unfolded state of low concentration STIM1 EF-SAM (~0.25 mg ml^{-1}) at 4 °C has been previously shown (28). *C*, urea-induced unfolding for STIM1 and STIM2 EF-SAM. Urea-induced unfolding (3.0 M) was monitored by changes in intrinsic fluorescence (arbitrary units (*a.u.*)) at 10 °C, 5 mM $CaCl_2$. Single exponential decay fits (*black lines*) showed no systematic deviation in the residuals over time. The *inset* shows the fitted unfolding rate constants for 0.0035 mg ml^{-1} STIM1 when compared with STIM2 EF-SAM over a range of urea concentrations at 10 °C.

STIM1 indicative of oligomerization (supplemental Fig. 1*A*); STIM2 demonstrated a much slower aggregation response to Ca^{2+} depletion (supplemental Fig. 1*B*).

Adjacent EF-SAM-flanking Residues Contribute to the N-terminal Stability of STIM Proteins—We investigated the effect of including all luminal residues on the stability of the constructs. Inclusion of residues 1–57 in the STIM1 EF-SAM construct (residues 58–201) yielded little recoverable protein, likely due to the hydrophobic nature of the ER signal peptide (residues 1–22); however, expression and purification of a construct encoding residues 23–213 was feasible. A STIM2 construct encompassing similar residue boundaries was susceptible to C-terminal degradation. Consequently, the long-N STIM2 construct was truncated at the C terminus (residues 15–205) to avoid the degradation issues.

The CD spectra of long-N STIM proteins (supplemental Fig. 2, *A* and *B*) display very similar spectral bands as the Ca^{2+}-loaded EF-SAM counterparts (27, 28). An important distinction is the intensity of the negative bands, where the long-N proteins yield less signal than EF-SAM normalized on a per residue basis (mean residue ellipticity); this difference implies that residues 23–57 for STIM1 and 15–61 for STIM2 adopt a considerable random coil character. Upon Ca^{2+} depletion of long-N STIM1, the intensity of the 222 nm band decreases markedly, whereas the 208 nm band decreases and is coupled with a shift to shorter wavelengths, indicative of increased overall random coil (supplemental Fig. 2*A*). The Ca^{2+} depletion-induced spectral changes for STIM2 are much more modest with only a small reduction in band intensity at both 208 nm and 222 nm (supplemental Fig. 2*B*). The Ca^{2+}-dependent conformational changes of the long-N constructs mimic those of the EF-SAM constructs (27, 28).

The stability of the long-N STIM constructs was assessed by monitoring changes in the CD signal at 225 nm as a function of temperature. The midpoint of the heat-induced loss in structure (T_{mid}) was ~59.5 °C in the presence of Ca^{2+} and ~37.5 °C in the Ca^{2+}-depleted state for STIM1 (supplemental Fig. 2*C*).

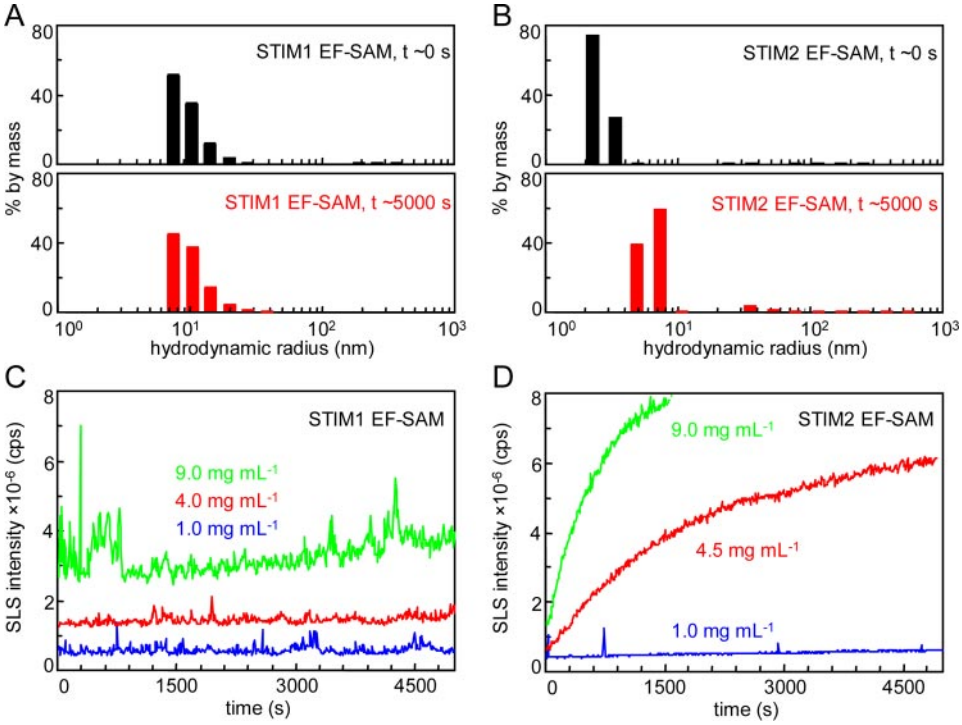

FIGURE 2. **STIM1 and STIM2 EF-SAM oligomerization kinetics.** *A*, regularization-deconvoluted DLS size distributions for STIM1 EF-SAM. Ca^{2+}-depleted samples were initially at 4 °C; DLS correlation functions (90°) were acquired as a function of time upon increasing the temperature to 25 °C. The mass-based distribution of hydrodynamic radii was indicative of oligomerized protein and did not change over the 5000-s time course at 4.0 mg ml^{-1}. *B*, regularization-deconvoluted DLS size distributions for STIM2 EF-SAM. Experiments were performed as per *A*. The mass-based distribution of radii underwent a monomeric-to-oligomeric transformation over 5000 s. *C*, the effect of protein concentration on the oligomerization rate of STIM1 EF-SAM. Changes in SLS intensity (90°) of Ca^{2+}-depleted protein were monitored as a function of time and concentration upon increasing the temperature from 4 to 25 °C. No systematic time-dependent change in SLS intensity (cps) at any protein concentration tested was observed for STIM1 EF-SAM. *D*, the effect of protein concentration on the oligomerization rate of STIM2 EF-SAM. Experiments were performed as per *C*. A time and protein concentration-dependent change in SLS intensity was observed for STIM2 EF-SAM.

These T_{mid} values for long-N STIM1 are ~14.5 and 16.5 °C higher than measured for Ca^{2+}-depleted and -loaded EF-SAM, respectively (27, 28). Similarly, the T_{mid} of long-N STIM2 in the absence and presence of Ca^{2+} was augmented by ~14.5 and 13.5 °C (supplemental Fig. 2*D*), respectively, when compared with the EF-SAM constructs (28). These data indicate that residues 23–57 for STIM1 and 15–61 for STIM2 have a marked stabilizing effect on the N-terminal of STIM proteins.

DISCUSSION

The role of STIM1 as an ER Ca^{2+} sensor that signals opening of Orai1-composed PM SOC channels is well established (4, 5, 7–9, 12, 14–18, 21, 24, 30). The function of STIM2 is more capricious; initial screening identified both STIM1 and STIM2 as positive regulators of SOCE (5). Follow-up studies indicated that STIM2 is an inhibitor of STIM1 punctae formation and SOCE (13). Subsequently, it was shown that STIM2-Orai1 co-overexpression constitutively activates SOCE (24). Both Ca^{2+}-independent as well as Ca^{2+}-sensing roles in SOCE activation were described, linking calmodulin as a subregulator of STIM2 function (25). More recently, STIM2 was reported as a regulator of basal cytoplasmic, and luminal Ca^{2+} levels via the Orai1 channel, where STIM2 Ca^{2+} sensing (*i.e.* Ca^{2+} depletion, oligomerization and ER-PM translocation) occurs at higher luminal Ca^{2+} levels than STIM1; moreover, depending on time and levels of expression, activating and inhibiting roles for STIM2 in SOCE were observed (26).

Our STIM1 EF-SAM solution structure afforded new insight into the basis for Ca^{2+} sensing by this luminal region; due to the high sequence similarity (*i.e.* >85%), an analogous structure can be inferred for STIM2 EF-SAM (12). Despite the probable gross structural mechanistic similarity between EF-SAM entities, here we reveal isoform distinctions at the kinetic level. STIM2 EF-SAM exhibits markedly decreased rates of oligomerization relative to STIM1. The observable concentration dependence in the CD and light scattering for STIM2 is consistent with this slower change in molecularity. Ca^{2+}-free STIM1 EF-SAM is directly unstructured and oligomeric, whereas STIM2 initially retains a well folded structure marginally different from the Ca^{2+}-loaded state. The presence of this stably folded state for STIM2 but not STIM1 (28) is the basis for the difference in the EF-SAM oligomerization dynamics. STIM1 EF-SAM undergoes rapid kinetic partial unfolding coupled with aggregation, whereas STIM2 exhibits markedly reduced, albeit concentration-dependent, rates of aggregation coupled to partial unfolding.

The slower aggregation kinetics and increased stability of STIM2 EF-SAM *versus* STIM1 may have contributed to the inconsistencies observed in cell culture (see above). The moderate stability of Ca^{2+}-depleted long-N STIM2 (T_{mid} ~50.5 °C) may allow oligomerization to be influenced by the relative membrane-tethered concentration, temperature, pH, pressure, and/or osmolytes; destabilizing factors could facilitate an oligomeric fate, whereas stabilizing phenomena could curtail STIM2-mediated SOCE initiation. Concentration, due to differing cell type or approaches in manipulating expression (*i.e.* transient, stable, or knockdown), and temperature (*i.e.* uncontrolled ambient) are examples of variable factors among the published STIM2 studies; relatively high concentrations and temperatures may promote SOCE, whereas lower levels and the potential ability of STIM2 to interact with STIM1 (see below) may inhibit SOCE (24). The marginal stability of Ca^{2+}-depleted long-N STIM1 (T_{mid} ~human physiological temperature) may render the oligomerization fate undeviating if the magnitude of stabilizing phenomena cannot overcome the degree of Ca^{2+} depletion-induced destabilization.

The long-N construct data reveal that the entire luminal sequence of STIM proteins influences the stability of the EF-hand-SAM domain interaction critical to Ca^{2+} sensing (12). There is large interspecies sequence variability beyond the EF-SAM entities (Fig. 1*A*); fine-tuning of STIM sensory function

may be encoded in these extraneous N-terminal residues. For example, STIM1 from *Drosophila melanogaster*, *Gallus gallus*, and *Caenorhabditis elegans* all encode vastly different luminal portions beyond EF-SAM. The STIM luminal portion of *D. melanogaster* is extensively longer than both human isoforms, *C. elegans* encodes only the basic EF-SAM entity with 14 adjacent residues, and *G. gallus* is truncated to the canonical EF-hand loop (non-confirmed). These distinctions may contribute to hypothetical differences in sensory characteristics between all isoforms, as observed for STIM1 *versus* STIM2 (see above) and *C. elegans* STIM1 *versus* mammalian STIM1 (31).

The evolution of STIM1 to rapidly oligomerize via EF-SAM facilitates a prompt conversion from a quiescent to a signaling state. A decreased Ca^{2+} sensitivity has been proposed for STIM2; even a slightly lower Ca^{2+} affinity in STIM2 when compared with STIM1 would promote considerably higher fractions of unbound STIM2 at resting ER Ca^{2+} levels (*i.e.* ~400 μM) (26). The persistent signaling of a low percentage of SOC channels would render the slower kinetics of EF-SAM oligomerization negligible and is consistent with a role for STIM2 in basal Ca^{2+} regulation (26). We propose that distinct dynamics of oligomerization (reported herein) have evolved in EF-SAM isoforms to foster discrete, yet harmonizing, signals. STIM1 (marginal stability/rapid oligomerization) delivers a quick SOCE regulatory signal, relatively large in magnitude and insusceptible to local factors that affect stability; STIM2 (moderate stability/protracted oligomerization) provides persistent SOC channel activation and a lower scale SOCE signal, which is responsive to local environmental influences. Recent work on T-cells from STIM knock-out mice supports the notion of a requisite role for both mammalian isoforms in SOCE despite considerably lower levels of STIM2 expression than STIM1 in the same cells (32). Ablation of STIM2 expression in these T-cells did not severely impair SOCE as observed for STIM1; nonetheless, a marked loss in cytokine production and decrease in nuclear factor of activated T-cells translocation demonstrated an essential role for STIM2 in these SOCE signaling events (32).

There are limited data on cross-talk between STIM isoforms (11, 13). Nonetheless, it is interesting to speculate that STIM1-STIM2 associations could provide additional regulatory control over SOCE and influence ER stress-related phenomena dependent on luminal Ca^{2+} depletion such as the unfolded protein response (33, 34). STIM2 would presumably stimulate the unfolded protein response to a lesser extent than STIM1 due to the higher EF-SAM stability and could co-stabilize STIM1 through potential heterotypic interactions. Additional studies are needed to further establish the functional roles of all STIM isoforms in SOCE and other cellular processes.

REFERENCES

1. Berridge, M. J., Bootman, M. D., and Roderick, H. L. (2003) *Nat. Rev. Mol. Cell Biol.* **4,** 517–529
2. Putney, J. W., Jr. (1986) *Cell Calcium* **7,** 1–12
3. Putney, J. W., Jr. (2007) *J. Cell Sci.* **120,** 1959–1965
4. Roos, J., DiGregorio, P. J., Yeromin, A. V., Ohlsen, K., Lioudyno, M., Zhang, S., Safrina, O., Kozak, J. A., Wagner, S. L., Cahalan, M. D., Velicelebi, G., and Stauderman, K. A. (2005) *J. Cell Biol.* **169,** 435–445
5. Liou, J., Kim, M. L., Heo, W. D., Jones, J. T., Myers, J. W., Ferrell, J. E., Jr., and Meyer, T. (2005) *Curr. Biol.* **15,** 1235–1241
6. Yeromin, A. V., Zhang, S. L., Jiang, W., Yu, Y., Safrina, O., and Cahalan, M. D. (2006) *Nature* **443,** 226–229
7. Vig, M., Peinelt, C., Beck, A., Koomoa, D. L., Rabah, D., Koblan-Huberson, M., Kraft, S., Turner, H., Fleig, A., Penner, R., and Kinet, J. P. (2006) *Science* **312,** 1220–1223
8. Vig, M., Beck, A., Billingsley, J. M., Lis, A., Parvez, S., Peinelt, C., Koomoa, D. L., Soboloff, J., Gill, D. L., Fleig, A., Kinet, J. P., and Penner, R. (2006) *Curr. Biol.* **16,** 2073–2079
9. Prakriya, M., Feske, S., Gwack, Y., Srikanth, S., Rao, A., and Hogan, P. G. (2006) *Nature* **443,** 230–233
10. Feske, S., Gwack, Y., Prakriya, M., Srikanth, S., Puppel, S. H., Tanasa, B., Hogan, P. G., Lewis, R. S., Daly, M., and Rao, A. (2006) *Nature* **441,** 179–185
11. Williams, R. T., Manji, S. S., Parker, N. J., Hancock, M. S., Van Stekelenburg, L., Eid, J. P., Senior, P. V., Kazenwadel, J. S., Shandala, T., Saint, R., Smith, P. J., and Dziadek, M. A. (2001) *Biochem. J.* **357,** 673–685
12. Stathopulos, P. B., Zheng, L., Li, G. Y., Plevin, M. J., and Ikura, M. (2008) *Cell* **135,** 110–122
13. Soboloff, J., Spassova, M. A., Hewavitharana, T., He, L. P., Xu, W., Johnstone, L. S., Dziadek, M. A., and Gill, D. L. (2006) *Curr. Biol.* **16,** 1465–1470
14. Zhang, S. L., Yu, Y., Roos, J., Kozak, J. A., Deerinck, T. J., Ellisman, M. H., Stauderman, K. A., and Cahalan, M. D. (2005) *Nature* **437,** 902–905
15. Wu, M. M., Buchanan, J., Luik, R. M., and Lewis, R. S. (2006) *J. Cell Biol.* **174,** 803–813
16. Luik, R. M., Wu, M. M., Buchanan, J., and Lewis, R. S. (2006) *J. Cell Biol.* **174,** 815–825
17. Liou, J., Fivaz, M., Inoue, T., and Meyer, T. (2007) *Proc. Natl. Acad. Sci. U. S. A.* **104,** 9301–9306
18. Mercer, J. C., Dehaven, W. I., Smyth, J. T., Wedel, B., Boyles, R. R., Bird, G. S., and Putney, J. W., Jr. (2006) *J. Biol. Chem.* **281,** 24979–24990
19. Spassova, M. A., Soboloff, J., He, L. P., Xu, W., Dziadek, M. A., and Gill, D. L. (2006) *Proc. Natl. Acad. Sci. U. S. A.* **103,** 4040–4045
20. Baba, Y., Hayashi, K., Fujii, Y., Mizushima, A., Watarai, H., Wakamori, M., Numaga, T., Mori, Y., Iino, M., Hikida, M., and Kurosaki, T. (2006) *Proc. Natl. Acad. Sci. U. S. A.* **103,** 16704–16709
21. Luik, R. M., Wang, B., Prakriya, M., Wu, M. M., and Lewis, R. S. (2008) *Nature* **454,** 538–542
22. Huang, G. N., Zeng, W., Kim, J. Y., Yuan, J. P., Han, L., Muallem, S., and Worley, P. F. (2006) *Nat. Cell Biol.* **8,** 1003–1010
23. Li, Z., Lu, J., Xu, P., Xie, X., Chen, L., and Xu, T. (2007) *J. Biol. Chem.* **282,** 29448–29456
24. Soboloff, J., Spassova, M. A., Tang, X. D., Hewavitharana, T., Xu, W., and Gill, D. L. (2006) *J. Biol. Chem.* **281,** 20661–20665
25. Parvez, S., Beck, A., Peinelt, C., Soboloff, J., Lis, A., Monteilh-Zoller, M., Gill, D. L., Fleig, A., and Penner, R. (2007) *FASEB J.* **22,** 752–761
26. Brandman, O., Liou, J., Park, W. S., and Meyer, T. (2007) *Cell* **131,** 1327–1339
27. Stathopulos, P. B., Li, G. Y., Plevin, M. J., Ames, J. B., and Ikura, M. (2006) *J. Biol. Chem.* **281,** 35855–35862
28. Zheng, L., Stathopulos, P. B., Li, G. Y., and Ikura, M. (2008) *Biochem. Biophys. Res. Commun.* **369,** 240–246
29. Cai, X. (2007) *PLoS ONE* **2,** e609
30. Peinelt, C., Vig, M., Koomoa, D. L., Beck, A., Nadler, M. J., Koblan-Huberson, M., Lis, A., Fleig, A., Penner, R., and Kinet, J. P. (2006) *Nat. Cell Biol.* **8,** 771–773
31. Gao, S., Fan, Y., Chen, L., Lu, J., Xu, T., and Xu, P. (2008) *Cell Calcium*, in press
32. Oh-hora, M., Yamashita, M., Hogan, P. G., Sharma, A., Lamperti, E., Chung, W., Prakriya, M., Feske, S., and Rao, A. (2008) *Nat. Immunol.* **9,** 432–443
33. Chen, L. H., Jiang, C. C., Kiejda, K. A., Wang, Y. F., Thorne, R. F., Zhang, X. D., and Hersey, P. (2007) *Carcinogenesis* **28,** 2328–2336
34. Yan, X., Xing, J., Lorin-Nebel, C., Estevez, A. Y., Nehrke, K., Lamitina, T., and Strange, K. (2006) *J. Gen. Physiol.* **128,** 443–459
35. Bendtsen, J. D., Nielsen, H., von Heijne, G., and Brunak, S. (2004) *J. Mol. Biol.* **340,** 783–795